ResearchGate

See discussions, stats, and author profiles for this publication at: https://www.researchgate.net/publication/8996965

DNA-Templated Carbon Nanotube Field-Effect Transistor

Article *in* Science · December 2003

DOI: 10.1126/science.1091022 · Source: PubMed

CITATIONS
780

READS
667

5 authors, including:

Kinneret Keren
Technion - Israel Institute of Technology
82 PUBLICATIONS **4,627** CITATIONS

SEE PROFILE

All content following this page was uploaded by Kinneret Keren on 30 June 2015.

The user has requested enhancement of the downloaded file.

EXTENDED PDF FORMAT
SPONSORED BY

BIO-RAD

http://discover.bio-rad.com

DNA-Templated Carbon Nanotube Field-Effect Transistor

Kinneret Keren, *et al.*

Science **302**, 1380 (2003);
DOI: 10.1126/science.1091022

The following resources related to this article are available online at www.sciencemag.org (this information is current as of April 10, 2007):

Updated information and services, including high-resolution figures, can be found in the online version of this article at:
http://www.sciencemag.org/cgi/content/full/302/5649/1380

Supporting Online Material can be found at:
http://www.sciencemag.org/cgi/content/full/302/5649/1380/DC1

This article **cites 26 articles**, 6 of which can be accessed for free:
http://www.sciencemag.org/cgi/content/full/302/5649/1380#otherarticles

This article has been **cited by** 154 article(s) on the ISI Web of Science.

This article has been **cited by** 5 articles hosted by HighWire Press; see:
http://www.sciencemag.org/cgi/content/full/302/5649/1380#otherarticles

This article appears in the following **subject collections**:
Physics, Applied
http://www.sciencemag.org/cgi/collection/app_physics

Information about obtaining **reprints** of this article or about obtaining **permission to reproduce this article** in whole or in part can be found at:
http://www.sciencemag.org/about/permissions.dtl

Downloaded from www.sciencemag.org on April 10, 2007

Science (print ISSN 0036-8075; online ISSN 1095-9203) is published weekly, except the last week in December, by the American Association for the Advancement of Science, 1200 New York Avenue NW, Washington, DC 20005. Copyright c 2003 by the American Association for the Advancement of Science; all rights reserved. The title SCIENCE is a registered trademark of AAAS.

DNA-Templated Carbon Nanotube Field-Effect Transistor

Kinneret Keren,[1] Rotem S. Berman,[1] Evgeny Buchstab,[2] Uri Sivan,[1,2] Erez Braun[1,2]*

The combination of their electronic properties and dimensions makes carbon nanotubes ideal building blocks for molecular electronics. However, the advancement of carbon nanotube–based electronics requires assembly strategies that allow their precise localization and interconnection. Using a scheme based on recognition between molecular building blocks, we report the realization of a self-assembled carbon nanotube field-effect transistor operating at room temperature. A DNA scaffold molecule provides the address for precise localization of a semiconducting single-wall carbon nanotube as well as the template for the extended metallic wires contacting it.

Individual single-wall carbon nanotubes (SWNT) have been used to realize molecular-scale electronic devices such as single-electron (*1*) and field-effect transistors (FET) (*2*). Several SWNT-based devices have been successfully integrated into logic circuits (*3*) and transistor arrays (*4*). However, the difficulty in precise localization and interconnection of nanotubes impedes further progress toward larger-scale integrated circuits.

Self-assembly based on molecular recognition provides a promising approach for constructing complex architectures from molecular building blocks, such as SWNTs, bypassing the need for precise nanofabrication and mechanical manipulations (*5*). Biology, with its inherent self-assembly capabilities (*6*–*13*), is particularly attractive for this task. Biological recognition has been imparted to carbon nanotubes (*14*–*18*), but their self-assembly into functional devices and circuits has not yet been demonstrated. We present a framework for self-assembly of carbon nanotube–based electronics using DNA and homologous genetic recombination. A semiconducting SWNT was localized at a desired address on a DNA scaffold molecule using homologous recombination by the RecA protein from *Escherichia coli* bacteria (*19*). DNA metallization, with the RecA doubling as a sequence-specific resist (*13*), led to the formation of extended conductive wires that electrically contact the SWNT. The conduction through the SWNT was controlled by a voltage applied to the substrate supporting the structure.

The SWNT-FET (Fig. 1) was assembled via a three-strand homologous recombination reaction between a long double-stranded DNA (dsDNA) molecule serving as a scaffold and a short, auxiliary single-stranded DNA (ssDNA) (*20*). The assembly process was guided by the information encoded in these DNA molecules. The short ssDNA molecule was synthesized so that its sequence is identical to the dsDNA at the designated location of the FET. RecA proteins were first polymerized on the auxiliary ssDNA molecules to form nucleoprotein filaments (Fig. 1, step i), which were then mixed with the scaffold dsDNA molecules. A nucleoprotein filament bound a dsDNA molecule according to the sequence homology between the ssDNA and the designated address on the dsDNA (Fig. 1, step ii). The RecA later helped localize a SWNT at that address and protect the covered DNA segment against metallization (*13*). Figure 2A displays an atomic force microscope (AFM) image of a 500-base-long (~0.25 μm) ssDNA/RecA nucleoprotein filament bound to the homologous section in the middle of a 48,502 base pair long (~16 μm) λ-DNA molecule.

A streptavidin-functionalized SWNT was guided to the right location on the scaffold dsDNA molecule using antibodies to the bound RecA and biotin-streptavidin–specific binding (*20*) (Fig. 1, step iii), and the SWNTs were solubilized in water by micellization in SDS (*21*). The solubilized SWNTs were functionalized with streptavidin by nonspecific adsorption (*15*, *16*). Fluorescence microscopy of SWNTs with fluorescently labeled streptavidin indicates homogeneous coverage of the nanotubes with streptavidin. Primary antibodies to RecA were reacted with the product of the homologous recombination reaction, resulting in specific binding of the antibodies to the RecA nucleopro-

[1]Department of Physics, [2]Solid State Institute, Technion-Israel Institute of Technology, Haifa 32000, Israel.

*To whom correspondence should be addressed. E-mail: erez@physics.technion.ac.il

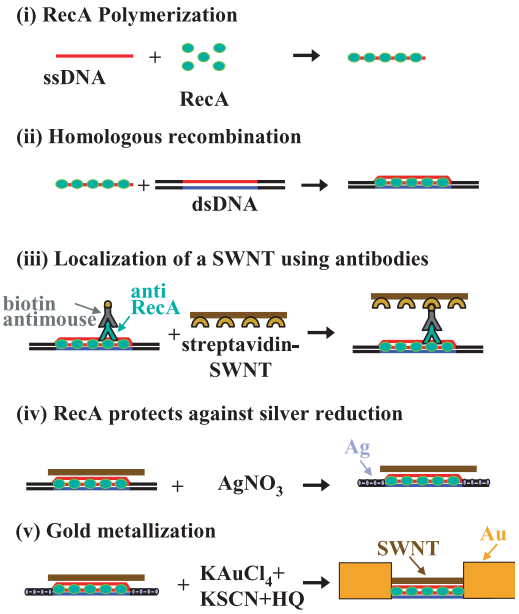

Fig. 1. Assembly of a DNA-templated FET and wires contacting it. Steps are as follows: (i) RecA monomers polymerize on a ssDNA molecule to form a nucleoprotein filament. (ii) Homologous recombination reaction leads to binding of the nucleoprotein filament at the desired address on an aldehyde-derivatized scaffold dsDNA molecule. (iii) The DNA-bound RecA is used to localize a streptavidin-functionalized SWNT, utilizing a primary antibody to RecA and a biotin-conjugated secondary antibody. (iv) Incubation in an $AgNO_3$ solution leads to the formation of silver clusters on the segments that are unprotected by RecA. (v) Electroless gold deposition, using the silver clusters as nucleation centers, results in the formation of two DNA-templated gold wires contacting the SWNT bound at the gap.

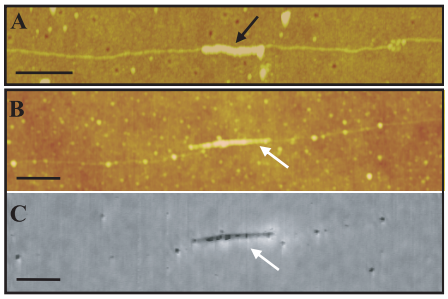

Fig. 2. Localization of a SWNT at a specific address on the scaffold dsDNA molecule using RecA. (**A**) An AFM image of a 500-base-long (~250 nm) RecA nucleoprotein filament (black arrow) localized at a homologous sequence on a λ = DNA scaffold molecule. Bar, 200 nm. (**B**) An AFM image of a streptavidin-coated SWNT (white arrow) bound to a 500-base-long nucleoprotein filament localized on a λ-DNA scaffold molecule. Bar, 300 nm. (**C**) A scanning conductance image of the same region as in (B). The conductive SWNT (white arrow) yields a considerable signal whereas the insulating DNA is hardly resolved. Bar, 300 nm. Phase shift limits, 0° to 20° (*20*).

Downloaded from www.sciencemag.org on April 10, 2007

tein filament. Next, biotin-conjugated secondary antibodies, which have high affinity to the primary ones, were localized on the primary antibodies to RecA. Finally, the streptavidin-coated SWNTs were added, leading to their localization on the RecA via biotin-streptavidin–specific binding (Fig. 1, step iii). The DNA/SWNT assembly was then stretched on a passivated oxidized silicon wafer (*20*). An AFM image of a SWNT bound to a RecA-coated 500-base-long ssDNA localized at the homologous site in the middle of a scaffold λ-DNA molecule is shown (Fig. 2B). The conducting carbon nanotube is distinguished from the insulating DNA by scanning conductance microscopy (*22*, *23*). Figure 2, B and C, depicts topographic and conductance images, respectively, of the same area. The evident difference between the two images identifies the SWNT on the DNA molecule; the carbon nanotube is aligned with the DNA, which is almost always the case due to the stiffness of the SWNT and the stretching process. In rare cases (<5%), we find misaligned SWNTs bound to the RecA (fig. S1). In certain cases, we find ropes rather than single nanotubes, due to the difficulty in achieving stable suspensions of individual SWNTs in an aqueous solution (*20*).

After stretching on the substrate, the scaffold DNA molecule is metallized (*20*). The RecA, doubling as a sequence-specific resist, protects the active area of the transistor against metallization. We used a previously developed metallization scheme (*13*) in which aldehyde residues, acting as reducing agents, are bound to the scaffold DNA molecules by reacting the latter with glutaraldehyde. The aldehyde derivatization, done before the homologous recombination reaction, was shown to be compatible with the whole process (*13*). Highly conductive metallic wires were formed by silver reduction along the exposed parts of the aldehyde-derivatized DNA (Fig. 1, step iv) and subsequent electroless gold plating (*20*), using the silver clusters as nucleation centers (Fig. 1, step v). Because the SWNT is longer than the gap dictated by the RecA, the deposited metal covers the ends of the nanotube and makes contact with it. Figure 3A depicts a scanning electron microscope (SEM) image of an individual SWNT contacted by two DNA-templated gold wires. The scaffold DNA molecule and the RecA are not resolved by the SEM.

The DNA-templated gold wires are contacted by e-beam lithography, and the device is characterized by direct electrical measurements under ambient conditions. Schematics of the measurement circuit and the electronic characteristics of the device are shown in Fig. 4. The gating polarity indicates p-type conduction of the SWNT, as is usually the case with semiconducting carbon nanotubes in air (*24*). The saturation of the drain-source current for negative gate voltages indicates resistance in series with the SWNT. The resistance is attributed to the contacts between the gold wires and the SWNT because the resistance of the DNA-templated gold wires is typically smaller than 100 Ω (*13*). Large-scale circuits will require better contacts (*20*). In some cases, the FET comprises nanotube ropes. These can be identified by their larger contrast in SEM imaging (Fig. 3B). The rope devices cannot be turned off by gate voltage, probably due to the fact that they contain metallic nanotubes in parallel with the semiconducting ones; both types are present in our samples. The metallic nanotubes cannot be depleted by the available electric field. As the gate bias is made more positive, the rope conduction decreases but saturates to a finite value (fig. S2). Different devices have somewhat different turn-off voltages. They all exhibit hysteresis in the drain-source current as a function of gate bias (fig. S3). Similar behavior is observed in carbon nanotube FETs fabricated by top-down approaches (*25*). Overall, we measured 45 devices from 3 different batches. Fourteen devices functioned as FETs with partial or full gating, 10 devices conducted but could not be gated (probably metallic SWNT ones, see fig. S4), and the rest were mostly disconnected and sometimes shorted to the gate. Our samples contain a mixture of semiconducting and metallic SWNTs, a fact that limits the yield of functional FETs. This drawback can be mitigated by recently developed techniques for separating semiconducting SWNTs from metallic ones (*26*–*28*).

The realization of a SWNT FET in a test tube promotes self-assembly as a realistic strategy for the construction of carbon nanotube-based electronics. The approach developed here can be generalized, in principle, to form a functional circuit on a scaffold DNA network. Numerous molecular devices could be localized simultaneously at different addresses on the network and interconnected by DNA-templated wires (*12*). The RecA-based scheme is robust and general enough to allow flexibility in the integration of other active electronic components into circuits, as long as they are compatible with the biological reactions and the metallization process. Realization of a functional circuit will require improving the electronic properties of the transistor and individual gating to each device. The latter could be achieved by using a three-armed DNA junction as a template (*13*) with the SWNT localized at the junction and by developing a method for turning one of the arms into a gate.

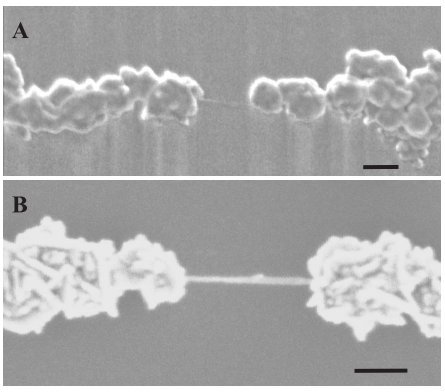

Fig. 3. A DNA-templated carbon nanotube FET and metallic wires contacting it. SEM images of SWNTs contacted by self-assembled DNA-templated gold wires. (**A**) An individual SWNT. (**B**) A rope of SWNTs. Bars, 100 nm.

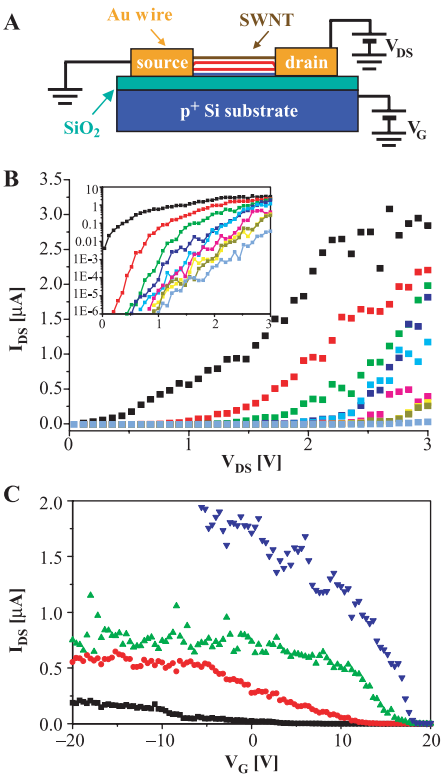

Fig. 4. Electrical characteristics of the DNA-templated carbon nanotube FET. (**A**) Schematic representation of the electrical measurement circuit. (**B**) Drain-source current (I_{DS}) versus drain-source bias (V_{DS}) for different values of gate bias (V_G). V_G = –20 V (black), –15 V (red), –10 V (green), –5 V (blue), 0 V (cyan), 5 V (magenta), 10 V (yellow), 15 V (olive), 20 V (slate blue). The inset depicts the same data on a logarithmic scale. (**C**) Drain-source current versus gate voltage for different values of drain-source bias [same device as (B)]. V_{DS} = 0.5 V (black), 1 V (red), 1.5 V (green), 2 V (blue).

References and Notes

1. H. W. Ch. Postma, T. Teepen, Z. Yao, M. Grifoni, C. Dekker, *Science* **293**, 76 (2001).
2. S. J. Tans, A. R. M. Verschueren, C. Dekker, *Nature* **393**, 49 (1998).
3. A. Bachtold, P. Hadley, C. Dekker, *Science* **294**, 1317 (2001).
4. A. Javey, Q. Wang, A. Ural, Y. Li, H. Dai, *Nano Letters* **2(9)**, 929 (2002).

Downloaded from www.sciencemag.org on April 10, 2007

5. J. R. Heath, M. A. Ratner, *Phys. Today* **2003**, 43 (May 2003).
6. N. Seeman, *Nature* **421**, 427 (2003).
7. C. A. Mirkin, R. L. Letsinger, R. C. Mucic, J. J. Storhoff, *Nature* **382**, 607 (1996).
8. A. P. Alivisatos *et al.*, *Nature* **382**, 609 (1996).
9. E. Winfree, F. Liu, L. A. Wenzler, N. C. Seeman, *Nature* **394**, 539 (1998).
10. C. Niemeyer, *Curr. Opin. Chem. Biol.* **4**, 609 (2000).
11. E. Braun, Y. Eichen, U. Sivan, G. Ben-Yoseph, *Nature* **391**, 775 (1998).
12. Y. Eichen, E. Braun, U. Sivan, G. Ben-Yoseph, *Acta Polym.* **49**, 663 (1998).
13. K. Keren *et al.*, *Science* **297**, 72 (2002).
14. K. A. Williams, P. T. M. Veenhuizen, B. G. de la Torre, R. Eritja, C. Dekker, *Nature* **420**, 761 (2002).
15. F. Balavoine *et al.*, *Angew. Chem. Int. Ed.* **38**, 1912 (1999).
16. M. Shim, N. W. S. Kam, R. J. Chen, Y. Li, H. Dai, *Nano Letters* **2(4)**, 285 (2002).
17. G. R. Dieckmann *et al.*, *J. Am. Chem. Soc.* **125**, 1770 (2003).
18. D. Pantarotto *et al.*, *J. Am. Chem. Soc.* **125**, 6160 (2003).
19. M. M. Cox, *Prog. Nucleic Acid Res. Mol. Biol.* **63**, 311 (2000).
20. Materials and Methods are available as supporting online material on *Science* Online.
21. J. Liu *et al.*, *Science* **280**, 1253 (1998).
22. C. Gomez-Navarro *et al.*, *Proc. Natl. Acad. Sci. U.S.A.* **99**, 8484 (2002).
23. M. Bockrath *et al.*, *Nano Letters* **2**, 187 (2002).
24. P. Avouris, *Acc. Chem. Res.* **35**, 1026 (2002).
25. K. Bradley, J. Cumings, A. Star, J. C. P. Gabriel, G. Grulner, *Nano Letters* **3**, 639 (2003).
26. R. Krupke, F. Hennrich, H. v. Lohneysen, M. M. Kappes, *Science* **301**, 344 (2003).
27. D. Chattopadhyay, I. Galeska, F. Papadimitrakopoulos, *J. Am. Chem. Soc.* **125**, 3370 (2003).
28. M. Zheng *et al.*, *Nature Mater.* **2**, 338 (2003).

29. We thank C. Dekker and K. Williams for helpful discussions regarding the attachment of streptavidin to nanotubes and for providing us with purified nanotube material suspended in SDS. We thank M. Konorty, Y. Cohen, Y. Dror, U. Banin, and Y. Ebenstein for help and discussions and N. Brenner for comments on the manuscript. The research was conducted in the Ben and Esther Rosenbloom Nanoelectronics by Biotechnology center of excellence. Research was supported by the Israeli Science Foundation and the Technion grant for promotion of research. K.K. acknowledges support by the Clore Foundation.

Supporting Online Material
www.sciencemag.org/cgi/content/full/302/5649/1380/DC1
Materials and Methods
Figs. S1 to S4
References

2 September 2003; accepted 15 October 2003

An Atomic-Level View of Melting Using Femtosecond Electron Diffraction

Bradley J. Siwick, Jason R. Dwyer, Robert E. Jordan, R. J. Dwayne Miller

We used 600-femtosecond electron pulses to study the structural evolution of aluminum as it underwent an ultrafast laser–induced solid-liquid phase transition. Real-time observations showed the loss of long-range order that was present in the crystalline phase and the emergence of the liquid structure where only short-range atomic correlations were present; this transition occurred in 3.5 picoseconds for thin-film aluminum with an excitation fluence of 70 millijoules per square centimeter. The sensitivity and time resolution were sufficient to capture the time-dependent pair correlation function as the system evolved from the solid to the liquid state. These observations provide an atomic-level description of the melting process, in which the dynamics are best understood as a thermal phase transition under strongly driven conditions.

Solid-liquid phase transitions are an everyday occurrence. As one of the state variables (such as temperature or pressure) approaches a phase transition point for the melting of a solid, there are equilibrium fluctuations that lead to density changes commensurate with the new phase. Fluctuations important to a collective phase transition under these conditions occur over distributed time and length scales in which the atomic details are washed out. By using short-pulsed lasers to deposit heat at a rate faster than the thermal expansion rate, it is possible to prepare extreme states of solid matter at temperatures well above the normal melting point (this will be referred to as the strongly driven limit). Under such conditions, the atomic configuration of the entire excited material volume can be modified on the ultrafast time scale, and the melting transition of the prepared state can be seen as a simple model for transition state processes in general.

Departments of Chemistry and Physics, 80 St. George Street, University of Toronto, Toronto, Ontario, Canada M5S 3H6.

An atomistic view of such a process requires that the atomic configuration of the material be observed as it passes from the solid to the liquid state. Ideally, one would like to be able to fully resolve the relative atomic motions during the melting process. The information accessible through time-resolved diffraction experiments, where the observable is intimately connected with the atomic structure of the material (*1*), can approach such a description. The first experiment along these lines used electron diffraction combined with rapid laser heating, but lacked sufficient temporal resolution (20 to 100 ps) and structural sensitivity for an atomic-level perspective on the process (*2*). Important applications of time-resolved electron diffraction have recently provided atomic-level structural details of reactive intermediates in the gas phase occurring on a similar time scale (*3*–*5*). Approaches based on laser-driven x-ray plasma sources have provided improved temporal resolution (200 to 500 fs) but to date have an insufficient signal-to-noise ratio (structural sensitivity) to adequately resolve the atomic details (*6*–*8*). Here we describe an important advance in short-pulsed electron sources that has made it possible to attain femtosecond electron pulses with sufficient electron number density to study the structural evolution of aluminum (Al) as it undergoes an ultrafast laser-induced solid-liquid phase transition. This work gives an atomic-level perspective on one of the simplest transition state processes: the order-to-disorder phase transition involved in melting.

Previous studies of femtosecond laser irradiation of polycrystalline Al at high fluence have observed the onset of liquid-like dielectric properties within 500 fs after laser excitation (*9*). It was inferred that lattice melting had occurred on this time scale, which is shorter than the time required for the optically excited electrons in the solid to relax via lattice phonon scattering. A nonthermal mechanism for melting was thus proposed, wherein the lattice bonding softens because of the photoinduced changes in electron distribution. Similar observations have been made in other materials (*10*, *11*); however, it is not possible to determine detailed quantitative information about the nuclear coordinates from the electronic response (probed in optical measurements), especially for these far-from-equilibrium conditions. Time-resolved diffraction offers a direct probe of the atomic structure of polycrystalline and amorphous samples by providing, through a simple transformation, the time-dependent (atomic) pair correlation function. Such a measurement is able to determine how the lattice structure maps onto the disordered state defining a liquid. In the case of Al, we were able to follow the loss of the long-range order that was present in the crystalline phase and the emergence of the liquid structure where only short-range atomic correlations were present; the transition was complete within 3.5 ps for 20-nm-thick samples at an excitation fluence of 70 mJ/cm^2. As opposed to previous studies of strongly driven phase transitions, we were able to define the onset of the liquid state and found that even in the strong perturbation limit, the phase transition in Al is propagated by thermally sampled

Downloaded from www.sciencemag.org on April 10, 2007

View publication stats